

A 5-Axis Mini Direct Drive Robot for Time Delayed Teleoperation

Blake Hannaford, Pierre-Henry Marbot, Manuel Moreyra, Steven Venema

Dept. of Electrical Engineering FT-10

University of Washington

Seattle, WA 98195

blake@biorobotics.ee.washington.edu

ABSTRACT

A previously developed 3 axis mini direct drive robot has been enhanced with two additional direct drive axes for general positioning and orientation of an axially symmetric tool. The arm has a work volume of about 50 cc and will have 5-10 micron or better resolution and repeatability. The arm forms an initial prototype for the NASA/University of Washington MicroTrex flight telerobotics experiment. The contemplated terrestrial applications include handling sub-microliter liquid samples for electrophoresis, and micro-manipulation with scaled force reflection.

INTRODUCTION

In recent years teleoperation has greatly expanded its scope of applications from its beginnings in the nuclear industry and its early expansion into undersea operations. Space and terrestrial biomedical applications are now attracting increasing attention.

In both of these areas, in addition to the desirability of removing humans from sources of physical risk (the vacuum of space or highly infectious agents for example), there is increasing interest in miniaturization. In space, economic and other pressures are shifting the emphasis from relatively heavy, high cost and complex systems, towards low mass, low cost systems with fewer functions and higher launch frequency. In surgery, similar pressures are encouraging replacement of traditional operations with endoscopic ones which are much less invasive. In both space and medical applications, communication links and time delays will play a key role in the overall system design.

This paper will report on a new manipulator designed to explore the possibilities and challenges of small scale manipulation in these applications. The arm is a five axis direct drive design having a work volume of about 50 cc. The arm is designed as a prototype for use in the NASA Micro Telerobotics Flight Experiment, "MicroTrex".

Time Delay. Some time delay is unavoidable in the com-

munication links between master and slave manipulators in telemanipulation. If it is of sufficient magnitude, this delay effects both the control system dynamics and the human operator performance. The effects of time delays on telemanipulation performance have for the most part been well studied. For a recent review, see Hannaford (1994). One exception is the case of time varying delays. Variable delays characterize all of the existing communication channels between earth and low earth orbit. These channels were designed solely for reliable accumulation of telemetry and imaging data and were not designed to latency requirements.

Flight Experiments. The ROTEX experiment was conducted by Dr. Gerd Hirzinger in May of 1993 (Hirzinger, et.al., 1993). In this experiment, a human scaled, gear driven arm, flown in the Space-Lab D2 was successfully controlled from the Space-Lab flight deck, as well as from a ground control station.

The arm described in the present paper is a preliminary prototype being developed for the NASA Micro Telerobotics Experiment, MicroTrex. This joint experiment between the University of Washington and the Jet Propulsion Laboratory will launch a small robot manipulator into low earth orbit and control it from the ground to perform an end-to-end test of ground-based remote control of space robots. The robot will perform tasks designed to simulate key activities of future robotic missions. The long term aim of this experiment is to provide design information for future micro and full size telerobots which will be required for human exploitation of space. In the shorter term, results are expected to benefit users and maintainers of the Space Station as well as terrestrial domestic biotechnology researchers and industries. A real-time video link to local schools is planned to make MicroTrex an educational and motivational experience for future engineers. Currently, MicroTrex has been approved for Phase-A funding under the NASA In Space Technology Experiments Program (INSTEP).

Direct Drive Robots. DD robots have several advantages for manipulation including high precision and high speed (Asada & Kanade, 1983, Asada & Youcef-Toumi, 1987). Most of the previous research in direct drive robots has concerned manipulators aimed at industrial applications and having work volumes on the order of human arms. Recently we have been studying the properties of direct drive robots with much smaller dimensions. In earlier work (Marbot & Hannaford, 1991) we described a 3 axis direct drive manipulator with a work volume of about 30 cc, aimed at applications in manipulation of cells and very young embryos in the biomedical laboratory. This arm was also adapted for pick and place telemanipulation of small objects on the order of individual sand grains (Bhatti, et.al., 1992). For the current arm, we have redesigned and re-manufactured the first three links and have added 2 additional degrees of freedom.

We were able to obtain high performance actuators for the robot from computer hard disk drives. Voice coil and “flat coil” actuators, used for positioning the heads of disk drives, must meet many of the same design criteria as for direct drive robots, and are mass produced at low cost. Recently we have made detailed measurements of their performance (Buttolo et. al., 1994).

Laboratory Applications. Several potential biomedical applications drive this design. One is loading sub-microliter fluid samples onto miniaturized electrophoresis gels for isoelectric focusing analysis. This job will require precision placement of a micro-pipette into liquid sample vials as small as 2 mm. in diameter. We intend to experiment with collecting samples from high density (864 well) micro-titer plates (molded sample vial arrays). These new plates occupy the same space as a standard 96 well plate (82 by 125 mm.) with 9 times the well density. Accessing the wells will require 2 additional degrees of freedom beyond the original three since the pipette must be oriented along the major axis of the well. Arbitrary angles may be required to clear microscope objectives or other equipment. A sixth axis (“tool roll”) is not needed in this application due to the axial symmetry of the pipette.

The following sections will describe the Mini DD robot at its current state of development. First, the robot structure will be described and analyzed in terms of the kinematic model and Jacobian matrix. Then the control system will be described, and the current project status will be summarized.

MINI-ROBOT MECHANISM

The first axis actuator is a linear voice coil from a 5.25

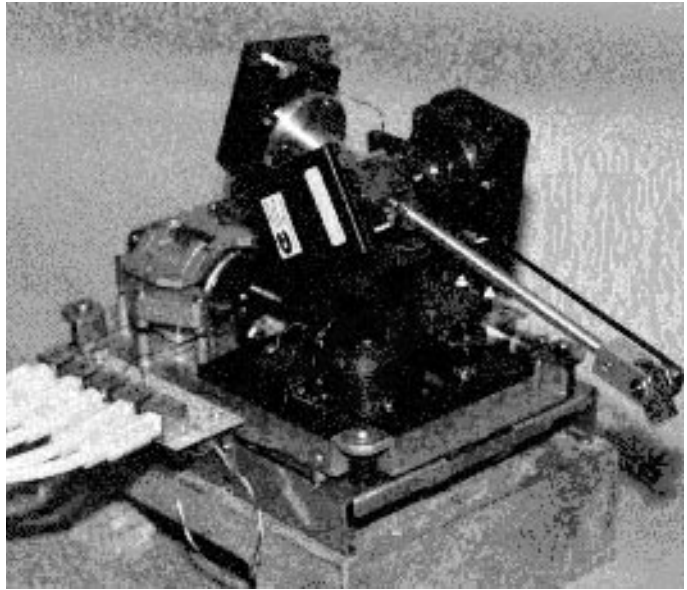


Figure 1
Photograph of the Mini Direct Drive Robot

inch hard disk drive. The second joint is driven by a rotary magnetic actuator. The third axis actuator is a rotary voice coil. The body of the mini-robot contains 20 individual parts machined of aluminum and anodized.

The original 3 axis design was modified in order to add two more degrees of freedom. Low inertia of the parts and high resolution and repeatability of the end effector displacements were design goals. The resulting mechanism allows generalized motion of the end-effector in five degrees of freedom: three displacements, and two rotations (pitch and yaw).

Biomedical applications, such as electrophoresis procedures and laboratory sample manipulation, were used as a guideline in the current development. An additional goal was to produce a device suitable to act as a slave manipulator for experiments in scaled force reflection (Colgate, 1991, Hannaford, 1991, Kobayashi & Nakamura, 1992). The project attempts to extend the technology of mini-robotics with several particular emphases:

- Employ direct drive actuation to maintain accuracy and repeatability, to enhance force control and to avoid backlash.
- Provide good dynamic performance by minimizing inertia.
- Use miniature disk-drive components, to get high precision, low inertia and low cost.

- Make the two orientation axes intersect at the wrist.

The electrophoresis sample handling procedure to be performed by the mini-robot consists of:

- Picking up 500 μ l and smaller protein samples from a well as small as two millimeters in diameter with a pipette attached to the wrist,
- Placing the sample on the electrophoresis gel,
- Washing and rinsing the pipette.

WORKSPACE DESIGN

The mini-robot workspace is reduced to an unusual extent by the limited range of the direct drive rotary actuators. Optimization of the performance of the mini-robot involved obtaining as large a work space as possible without compromising speed, force and precision of end effector movements. The work space chosen was approximately 75 mm. height, 25 mm. width and 25 mm. length. This will allow the robot to reach about 18 of the wells on a standard 96 well microtiter plate. This will be sufficient for the intended experimental applications.

The overall design of the first three axes is the same as reported earlier (Marbot & Hannaford, 1991). However, the parts were re-designed and re-machined to improve precision and to support the addition of two more motion axes. The same linear voice coil actuator was used for the first, linear motion axis. Two high accuracy, low friction linear ball bearings, also taken from disk drives, guide and support the first motion axis.

The second joint is driven by a rotary magnetic actuator. Its angular stroke is $\pm 15^\circ$ and the arm is 6" (152mm) long, giving a Y-axis travel of ± 1.55 " (± 40 mm.). The third axis actuator has angular stroke of $\pm 13^\circ$ giving a Z-axis travel of ± 1.35 " (± 34 mm.).

The fourth and fifth joints have $\pm 20^\circ$ of stroke. We do not consider them to affect work volume since they drive intersecting axes at the wrist. However, there is a minimum offset from wrist center to tool mount of 22 mm.. Due to the low torque of actuator 3 and the relatively high weight and size of the actuator and encoder used on the fifth joint, direct drive in the strict sense of the term is not used. Instead, a belt and two pulleys are used to drive this joint with a 1:1 mechanical advantage.

ACTUATORS

Table 1 shows the basic mechanical and electrical characteristics of the mini-robot actuators. The first axis actuator is a linear voice coil from a 5.25 inch hard disk drive. The second joint is driven by a rotary magnetic actuator (BEI Motion Systems Company). It has four coils in the rotor and four ceramic magnets. The peak torque is 11 oz.-in. (0.08 Nm) when the coils are aligned between the magnets. The torque vs. angle curve is equivalent to $\cos^2(2\theta_2)$. Its total weight is 3.6 Oz. (100gr). This actuator was not taken from a hard drive. In retrospect, this unit gave inferior performance at greater cost. A disk drive actuator would have had an almost constant torque-angle relation and lower mass.

The third axis actuator is a rotary actuator is also made by BEI (model No. RA23-06-001), but for a disk drive application. The moving member which includes the coil weighs 0.22 Oz. (6.3 gr.) and the total weight is 1.6 Oz. (46 gr.).

The fourth and fifth joints use head actuators from 1.8" disk drives. A minor alteration was made to the actuators so that they could drive a 0.25" (6.35 mm.) diameter shaft. Their weight is 0.7 oz. (20 gr) each.

Table 1: Performance data of Mini-Robot actuators.

Actuator	Stroke	Force or Torque Constant	Maximum Force or Torque	Coil Resistance Ohms	Current @ Maximum Cont. Load
1	25 mm.	2.5 N/Amp	5.0 N	3.4	2.0A
2	$\pm 15^\circ$	39×10^{-3} Nm/A	78×10^{-3} Nm	5.2	2.0 A
3	$\pm 13^\circ$	40×10^{-3} Nm/A	42×10^{-3} Nm	3.4	1.05 A
4	$\pm 20^\circ$	13.6×10^{-3} Nm/A	8.9×10^{-3} Nm	6.5	0.65 A
5	$\pm 20^\circ$	13.6×10^{-3} Nm/A	8.9×10^{-3} Nm	6.5	0.65 A

MINI-ROBOT KINEMATICS

The mini robot forward kinematic model is derived using the Denavit-Hartenberg convention and the frame definitions used in Craig (1991). Figure 2 depicts the schematic link diagram on which the kinematic analysis (Table 2) is based.

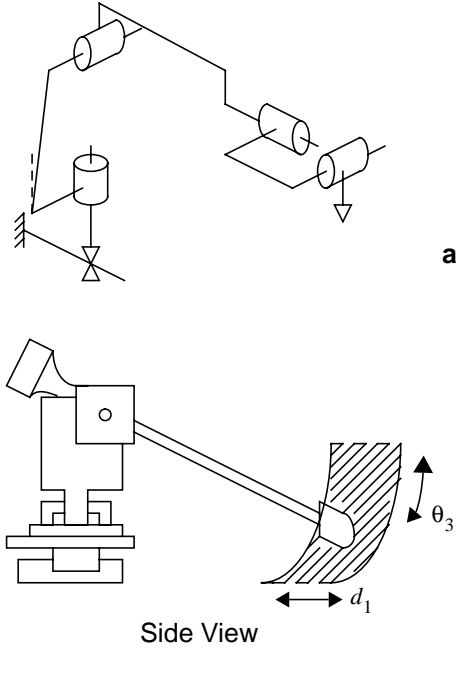


Fig.2

Mini robot schematic diagrams. Kinematic linkage diagram (a) and side view of mechanism and workspace (b)

Using the DH parameters from Table 1 and the standard procedure, we obtain:

$${}^0_5T = \begin{bmatrix} a_{11} & a_{12} & -c\theta_2c\theta_3s\theta_4 + s\theta_2c\theta_4 & -152c\theta_2s\theta_3 + 12.5c\theta_2 \\ a_{21} & a_{22} & s\theta_3s\theta_4 & -152c\theta_3 \\ a_{31} & a_{32} & s\theta_2c\theta_3s\theta_4 + c\theta_2c\theta_4 & 152s\theta_2s\theta_3 - 12.5s\theta_2 + d_1 \\ 0 & 0 & 0 & 1 \end{bmatrix} \quad (1)$$

where $c\theta_i = \cos\theta_i$, $s\theta_i = \sin\theta_i$, and

$$a_{11} = c\theta_2c\theta_3c\theta_4c\theta_5 + s\theta_2s\theta_4c\theta_5 + c\theta_2s\theta_3s\theta_5 \quad (2)$$

$$a_{12} = -c\theta_2c\theta_3c\theta_4s\theta_5 - s\theta_2s\theta_4s\theta_5 + c\theta_2s\theta_3c\theta_5 \quad (3)$$

$$a_{21} = -s\theta_3c\theta_4c\theta_5 + c\theta_3s\theta_5 \quad (4)$$

$$a_{22} = s\theta_3c\theta_4s\theta_5 + c\theta_3c\theta_5 \quad (5)$$

$$a_{31} = -s\theta_2c\theta_3c\theta_4c\theta_5 + c\theta_2s\theta_4c\theta_5 - s\theta_2s\theta_3s\theta_5 \quad (6)$$

$$a_{32} = s\theta_2c\theta_3c\theta_4s\theta_5 - c\theta_2s\theta_4s\theta_5 - s\theta_2s\theta_3c\theta_5 \quad (7)$$

INVERSE MINI-ROBOT KINEMATICS

Space precludes the full inverse kinematic solution in this paper. In this section we develop the problem in which the desired position of the wrist frame relative to the base frame $\{0\}$ is known, and we compute the joint position d_1 and angles θ_2 and θ_3 required to achieve this configuration.

We can equate the position to the last column of (2) giving

Table 2: Mini-robot Denavit-Hartenberg parameters.

i	a_{i-1} (degrees)	a_{i-1} (mm.)	d_i (mm.)	q_i (degrees)
1	0	0	$d_1 = \pm 12$	0
2	-90	0	0	$q_2 = -90 \pm 15$
3	-90	12.5	0	$q_3 = -60 \pm 13$
4	-90	0	152	$q_4 = 180 \pm 20$
5	-90	0	0	$q_5 = -120 \pm 20$

$${}^0P_{4ORG} = \begin{bmatrix} p_x \\ p_y \\ p_z \\ 1 \end{bmatrix} = \begin{bmatrix} -152 \cos \theta_2 \sin \theta_3 + 12.5 \cos \theta_2 \\ -152 \cos \theta_3 \\ 152 \sin \theta_2 \sin \theta_3 - 12.5 \sin \theta_2 + d_1 \\ 1 \end{bmatrix} \quad (8)$$

This yields the following expressions:

$$\theta_3 = \operatorname{atan2} \left(\frac{\left(1 - \left(\frac{p_y}{152} \right)^2 \right)^{\frac{1}{2}}}{\pm \left(\frac{p_y}{152} \right)} \right) \quad (9)$$

$$\theta_2 = \operatorname{atan2} \left(\frac{\left(1 - \left(\frac{p_x}{12.5 - 152 \sin \theta_3} \right)^2 \right)^{\frac{1}{2}}}{\pm \left(\frac{p_x}{12.5 - 152 \sin \theta_3} \right)} \right) \quad (10)$$

$$d_1 = p_z - 152 \sin \theta_2 \sin \theta_3 + 12.5 \sin \theta_2 \quad (11)$$

If joint angles were unrestricted, there would be four solutions. For the joint angles permitted by the limited actuator ranges, there is a unique solution, and $\operatorname{acos}()$ may be used in place of $\operatorname{atan2}()$ in (9) and (10) without the traditional difficulties (Craig, 1991).

JACOBIAN

The Jacobian matrix relates the joint rate to cartesian end effector velocity. It was computed using symbolic manipulation software developed earlier (Kung, et. al., 1992)

$${}^0J(\Theta) = \begin{bmatrix} 0 & a_{12} & -152 \cos \theta_2 \cos \theta_3 & 0 & 0 & 0 \\ 0 & 0 & 152 \sin \theta_3 & 0 & 0 & 0 \\ 1 & a_{32} & 152 \sin \theta_2 \cos \theta_3 & 0 & 0 & 0 \\ 0 & 0 & -\sin \theta_2 & -\cos \theta_2 \sin \theta_3 & a_{45} & 0 \\ 0 & 1 & 0 & -\cos \theta_3 & \sin \theta_3 \sin \theta_4 & 0 \\ 0 & 0 & -\cos \theta_2 & \sin \theta_2 \sin \theta_3 & a_{65} & 0 \end{bmatrix} \quad (12)$$

where

$$a_{12} = 152 \sin \theta_2 \sin \theta_3 - 12.5 \sin \theta_2 \quad (13)$$

$$a_{32} = 152 \cos \theta_2 \sin \theta_3 - 12.5 \cos \theta_2 \quad (14)$$

$$a_{45} = \sin \theta_2 \cos \theta_4 - \cos \theta_2 \cos \theta_3 \sin \theta_4 \quad (15)$$

$$a_{65} = \cos \theta_2 \cos \theta_4 + \sin \theta_2 \cos \theta_3 \sin \theta_4 \quad (16)$$

SENSORS

Most robots today use digital incremental position encoders to estimate joint positions. This works well when the mechanism design allows several turns of the encoder disk for small joint motions. However, the direct drive feature of the mini-robot, coupled with the desire for small, very high-precision motions, implies the need for different position measurement approaches.

LVDT Position sensor. For joint 1, a linear variable differential transformer (LVDT) is used. A specialized monolithic IC is used for the LVDT signal conditioning (Signetics NE5521). This chip provides an extremely stable amplitude/frequency source for the LVDT primary coil. In our implementation, a 12-bit A/D converter effectively limits the LVDT resolution to 1 part in 4096. The 1-inch travel of joint 1 therefore implies a position measurement precision of $0.0254m/2^{12} = 6.2\mu m$. This was verified in the earlier prototype by microscopic inspection of the axis displacement (Marbot & Hannaford, 1991).

Analog Incremental Encoders

Joints 2-5 are instrumented with analog incremental rotary position encoders. Unlike digital encoders, these encoders output two sinusoids in quadrature phase. These analog outputs allow a high degree of interpolation between each encoder line.

Determining actual angular position, θ_a from the sinusoidal outputs is a two stage process (Figure 3). First a

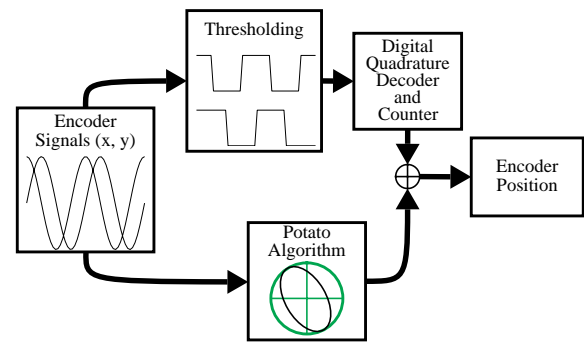


Figure 3: Analog Optical Encoder Signal Processing

coarse position, θ_c is maintained by passing a thresholded version of the sinusoids through a standard digital quadrature decoder/counter circuit. Like standard digital encoders, θ_c will have angular resolution equal to 4 times the

number of lines on the encoder disk. Expressed in units of encoder-lines, θ_c always yields positions that are multiples of 0.25.

The second stage of the process yields a finer resolution by using the relative amplitudes of the two sinusoids (called x and y) to compute a more accurate angular offset, θ_o from the closest encoder line. For an ideal encoder, x and y would be perfect sinusoids of identical magnitude and with exactly 90° relative phase difference. In this ideal case, the line offset position θ_o could be computed from the relation

$$\theta_o = \frac{\text{atan2}(y, x)}{2\pi} \quad (-0.5 \leq \theta_o < 0.5) \quad (17)$$

where $\text{atan2}()$ is the commonly used two-argument arctangent function. This offset position θ_o can then be combined with the digitally estimated position θ_c to yield an accurate estimate of the actual position θ_a :

$$\theta_a = \text{int}(\theta_c) + \theta_o + \begin{cases} 1 & \text{fract}(\theta_c) - \theta_o > \frac{1}{2} \\ -1 & \text{fract}(\theta_c) - \theta_o < -\frac{1}{2} \\ 0 & \text{otherwise} \end{cases} \quad (18)$$

θ_c is therefore corrected if the actual system, as measured by the analog outputs x , and y , is near the boundary of quadrants I and IV. This is accomplished by adding or subtracting 1 count to θ_c so that the error is propagated to the higher order bits.

However, the sinusoids from most analog encoders are far from ideal. Phase differences of 110° are not uncommon. When plotted against each other, these signals make an irregular potato-like shape instead of the expected perfect circle. The *potato algorithm* (Marbot, 1991) was developed to address these non-ideal behaviors of the encoder signals. Space limitations preclude more detailed treatment than appears below. For more details see (Marbot, 1991).

The Potato Algorithm

The potato algorithm models the encoder outputs as

$$\begin{aligned} x &= A \cos(\hat{\theta}_o) \\ y &= B \sin(\hat{\theta}_o - \Phi) \end{aligned} \quad (19)$$

where x and y are the quadrature outputs of the encoder, $\hat{\theta}_o$ is θ_o expressed in radians ($-\pi < \hat{\theta}_o < \pi$) is the actual joint position, A and B are the magnitudes of the quadrature signals, and Φ is the phase error between the two quadrature signals (nominally 0°). The potato algorithm uses this ellipsoidal approximation to map the

“potato” shape back onto the ideal circle.

If, for the moment, we only consider quadrants I and IV, solving (20) for $\hat{\theta}_o$ yields the relation,

$$\hat{\theta}_o = \text{atan}\left(\frac{Ay}{Bx \cos \Phi} + \tan \Phi\right) \quad (20)$$

In actual encoders, A and B tend to vary in a nearly identical manner due to the geometry of the light sensors. Note also from (21) that since Φ is a measured parameter of the encoder, $\cos(\Phi)$ and $\tan(\Phi)$ are constants in this equation. Therefore the computation only involves one multiply, one divide, one add, and one arctangent function. Since the two-argument arctangent function should be again used here, (21) can be rewritten as

$$\hat{\theta}_o = \text{atan2}(Ay + Bx \sin \Phi, Bx \cos \Phi) \quad (21)$$

Finally, $\hat{\theta}_o$ must be scaled into units of encoder lines using the relation,

$$\theta_o = \frac{\hat{\theta}_o}{\pi}. \quad (22)$$

Parameter Identification. In the original implementation of the potato algorithm, the parameters (A, B, Φ) were estimated off-line by moving the encoder at a constant velocity and sampling the encoder outputs at a high rate. The resulting data was then used to measure the amplitudes (A, B) and to estimate the quadrature phase error Φ .

Angular Resolution. The sinusoidal voltages go through their complete range twice in one encoder cycle. The 12-bit A/D converters used to sample x and y inherently limit the precision of the θ_o estimate to 1 part in 2^{12+1} or 0.000122 of an encoder line. For our 1000-line encoders, this implies a theoretical angular precision of

$$\frac{2\pi}{1000} \times \frac{1}{2^{13}} = 767 \times 10^{-9} \text{ radians}. \quad (23)$$

Since this mini-robot wrist is located 0.152m from the axis of rotation, the wrist position resolution is thus $116 \times 10^{-9} m$. This precision will undoubtedly be reduced by sensor noise and inaccuracies in the (A, B, Φ) parameters of the encoder model. Actual resolution has yet to be measured.

POWER ELECTRONICS

Most full-scale robots today are driven by pulse-width modulation (PWM) power electronics. The popularity of PWM is due primarily to its ability to control large amounts of power (up to several kilowatts per joint) with very high

efficiency. However, the high-speed current switching used in PWM systems generates a large amount of electromagnetic interference (EMI). Digital sensors (e.g., digital incremental encoders) can be made to operate robustly in this type of environment using good shielding and grounding techniques. However, to get less than 1-bit of noise on our analog to digital conversions, we must have a signal-to-noise ratio of better than 74dB. The amount of EMI generated by PWM power electronics makes it difficult to shield the encoder signals sufficiently to achieve this desired SNR.

Since the power levels needed to actuate the mini-robot are relatively small (~50 watts peak per actuator), we chose to use linear power amplifiers to drive the voice-coil actuators. High-power op-amps were configured as a voltage controlled current sources for each joint. D/A converters on our computer control system directly control the motor currents.

The design of the power electronics was constrained by two factors: (1) the range of actuator resistances (3.4 to 6.5Ω) and (2) the desired maximum current output (2 amps per actuator). These factors, in turn, determine the desired power supply voltage V_{cc} and the amount of heat sink area needed to keep the amplifiers' temperatures within their operating limits. The worst-case power dissipation is

$$P_{max} = \frac{V_{cc}^2}{2R_L} \quad (24)$$

where R_L is the resistance of the voice coil. The peak current output of the ideal op-amp is simply

$$I_{max} = \frac{V_{cc}}{R_L} \quad (25)$$

We selected a power supply voltage of 15 volts since this was the minimum supply voltage which would meet the 2-ampere criterion for the various actuator load resistances.

COMPUTER SYSTEM

A real-time digital computer system is used to control the mini-robot. The computer is an in-house design based upon Texas Instrument's TMS320C30 DSP chip. The processor consists of a 6U-VME form-factor circuit board containing the 32 MHz DSP chip, up to 256k 32-bit words of high speed SRAM, a special bus for communications with other processor boards, a daughter-card bus for the addition of peripheral cards, and an RS232-compatible

serial communications port for interface with an external host computer. Details of this design, including the processor's Neural Broadcast communications bus, can be found in MacDuff et.al, (1992).

The processor typically operates with a 16MHz instruction rate but supports a peak floating point throughput of 32MFLOPS using a two-stage instruction pipeline. Analog and digital I/O is accomplished using an add-on daughter card. Each daughter card contains 4 separate 33kHz 12-bit A/D and 12-bit D/A channels as well as 8 bits of digital input and 16 bits of digital output. Up to four daughter cards may be stacked on a single processor board.

Software is written in C and cross-compiled on Unix workstations using a compiler provided by Texas Instruments. We developed a ROM-monitor for the processor which supports downloading programs from the Unix workstations via the RS232 serial port. The end-to-end system configuration is shown in Figure 4.

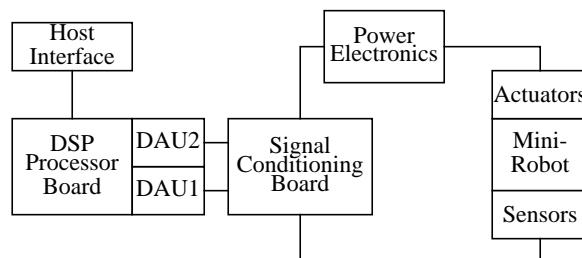


Figure 4: Control system block diagram.

CONCLUSION

The design of the UW mini direct drive robot has been described. The mechanics and electronics are now complete, and closed loop control has been demonstrated of each axis, employing the analog encoder signals. In work now underway, we will develop control methods for high performance and high precision point to point positioning. This will be required for the electrophoresis application. We plan to incorporate feed forward dynamic model information (Khosla, 1988) in the controller. In the second phase of the mini-robot development, we will study the control of contact forces in scaled teleoperation using the mini robot as a slave. Human control interface will be performed by a pen-based master device now approaching completion in our laboratory.

Finally, the mini robot forms the prototype for a small 6-axis manipulator for the MicroTrex space flight telerobotics experiment. The restricted motion range of the disk drive actuators provide a rather small workspace relative to the overall arm size. However, as with the original 3-axis prototype, this robot will be valuable for studying the control of small direct drive robots. For the eventual flight model, we expect to increase work volume by designing new actuators of greater motion range using proven design principles from disk drive actuators.

REFERENCES

- H. Asada, T. Kanade, "Design of Direct-Drive Mechanical Arms," ASME J. Vibration, Acoustics, Stress, and Reliability in Design, vol. 105, pp. 312-316, 1983.
- H. Asada, K. Youcef-Toumi, "Direct Drive Robots, Theory and Practice," MIT Press, Cambridge, MA, 1987.
- P. Bhatti, P.H. Marbot, B. Hannaford, "Microscopic Pick and Place with the Mini-Direct Drive Arm," SPIE Telemanipulation Symposium, Boston, November, 1992.
- P. Buttolo, D.Y. Hwang, B. Hannaford, "Experimental Characterization of Hard Disk Actuators for Mini Robotics," Proc. SPIE Telemanipulator and Telepresence Technologies Symposium, Boston, October, 1994.
- J.E. Colgate, "Power and Impedance Scaling in Bilateral Manipulation," Proc. IEEE Intl. Conf on Robotics and Automation, pp. 2292-2297, Sacramento, CA, 1991.
- J. Craig, "Introduction to Robotics: Mechanics and Control," Addison Wesley, 2nd Edition, 1991.
- B. Hannaford, "Ground Experiments towards Space Teleoperation with Time Delay," In-Press in "Manipulation, Automation, and Robotics in Space", S.B. Skaar, Ed., AIAA Press, 1994.
- G. Hirzinger, B. Brunner, J. Deitrich, J. Heindl, "Sensor-Based Space Robotics - ROTEX and its Telerobotic Features," IEEE Transactions on Robotics and Automation, v9, no 5., pp 649-663., 1993.
- P.K. Khosla, "Some Experimental Results on Model-Based Control Schemes," Proc. IEEE Intl. Conf. on Robotics and Automation, vol. 3, pp. 1380-1385, Philadelphia, PA, April 1988.
- H. Kobayashi, H. Nakamura, "A Scaled Teleoperation," Proc. IEEE Intl Workshop on Robot and Human Communication, pp. 269-274, Tokyo, 1-3 Sept. 1992.
- D. Kung, J. Parsons, B. Hannaford, "Visualization of Manipulability with Mathematica," Proceedings: IASTED Control & Robotics, Vancouver, August, 1992.
- I. MacDuff, S. Venema, B. Hannaford, "The Anthroform Neural Controller: A System for Detailed Emulation of Neural Circuits," Proceedings, IEEE International Conference on Systems, Man, and Cybernetics, Chicago, IL, September, 1992.
- P.H. Marbot, "Mini Direct Drive Robot for Biomedical Applications," MSEE Thesis, University of Washington, Department of Electrical Engineering, August, 1991.

ACKNOWLEDGEMENTS

We gratefully acknowledge the design assistance of Kevin Welton, and Tom Jackson, and donation of 1.8" head actuators by Dr. James Morehouse of Integral Peripherals Inc. Longmont Co. This research was supported by a National Science Foundation Presidential Young Investigator Award, and by the University of Washington Royalty Research Fund, and with equipment support from Texas Instruments Inc.